ACS OMEGA

http://pubs.acs.org/journal/acsodf

Article

Near-Infrared Turn-On Fluorescent Probe for Aqueous Fluoride Ion Detection and Cell Imaging

Yan Liu, Yaping Zhou, Hongyu Li,* Jie Gao, Mingyan Yang, Zeli Yuan,* and Xinmin Li*

Cite This: *ACS Omega* 2022, 7, 34317−34325

Read Online

ACCESS | Metrics & More | Article Recommendations | Supporting Information

ABSTRACT: Fluoride ions are one of the most essential anions in the human body and have been implicated in various pathological and physiological processes. The detection of fluoride ions in aqueous solution, as well as the imaging of fluoride ions in living cells, remains a challenge. We herein report a BODIPY-based fluorescent probe employing a pinacol borate group as the recognition moiety for the detection of fluoride ions in aqueous solutions. This probe shows high selectivity and sensitivity to fluoride ions with a significant near-infrared fluorescence turn-on response. In addition, this probe was successfully employed in fluorescence bioimaging of fluoride ions in the human cervical cancer cell and mouse mammary cancer cell, demonstrating its good cell permeability and stability under physiological conditions.

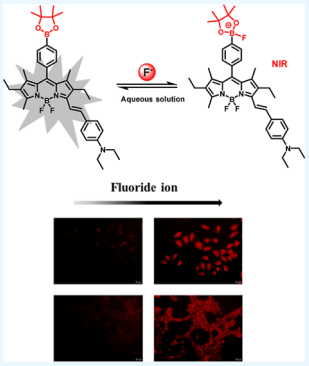

1. INTRODUCTION

Fluoride ion (F^-), the smallest anion,[1−3] is one of the essential trace elements which plays various roles in biochemical processes. Appropriate intake of fluoride is contributed to preventing dental cavities and osteoporosis.[4,5] However, excess fluoride ingestion can cause detrimental health effects and can calcify bone and teeth, resulting in various symptoms and diseases such as dental fluorosis, skeletal fluorosis, urolithiasis, and kidney failure.[6−10] Several analytical techniques, including ion chromatography, ion-selective electrodes, ultraviolet−visible spectroscopy, mass spectroscopy, and ^{19}F NMR, have been demonstrated for quantitative fluoride determination.[11−13] However, most of these methods have limitations, such as high experimental costs, tediousness, and time-consuming procedures, as well as inaccessibility for studying biological processes. Therefore, the development of a simple and highly sensitive method for F^- detection is still urgently needed. Compared with other analytical methods, fluorescence detection technology has attracted great attention as it has been proved to have simple techniques, cost-efficient experiments, high sensitivities, and selectivity and can also be applied to live cell imaging of anions.[14−16] Recently, several organic molecules have been reported as fluorescent probes for the detection of F^-.[17−22] These probes are based on the hydrogen bond mechanism where the O−H or N−H group is protonated or bonded under the action of fluorine, resulting in the change of molecular spectrum properties. However, since F^- is the most electronegative anion, it can also readily form hydrogen bonds with water molecules, which severely limits the detection of F^- in aqueous systems by hydrogen-bonded fluorescent probes. To overcome the issue of detecting F^- in aqueous solutions, a series of probes based on fluorine−boron complexation have been developed during the last few years.[23−28] The mechanism of such probes is based on the Lewis acid−base interactions. Since the boron atom has an empty p orbital, the electron-deficient trivalent organic boron readily binds to F^-, thus breaking the p-π conjugation of the boron center to the aromatic group, leading to a change in the photophysical properties of the probe molecule and thus achieving selective detection of F^-. The molecular probe based on the second mechanism is not affected by the aqueous solution, which can be used to detect F^- in vivo and in cells with high sensitivity and selectivity.

Near-infrared (NIR) fluorescent probes have great advantages for in vivo imaging because of their low background interference, low light source energy, high tissue penetration depth, low tissue damage, and high image sensitivity.[29,30] A series of fluorescent probes have been reported for detecting F^- in the last decade (Table S1), but fewer probes can be used as a sensitive NIR fluorescent turn-on sensor to detect F^-. In recent years, considerable progress has been reported for NIR fluorescent F^- probes based on rhodamine,[31] coumarin,[32] and hemicyanine structures;[33,34] however, achieving high sensitivity and selective F^- detection in aqueous solutions and living cells remains a challenge.[16,35−37] In this work, we have designed and

Received: June 21, 2022
Accepted: September 2, 2022
Published: September 12, 2022

Scheme 1. BODIPY-Based Turn-On Fluorescent Probe for the Detection of F^-

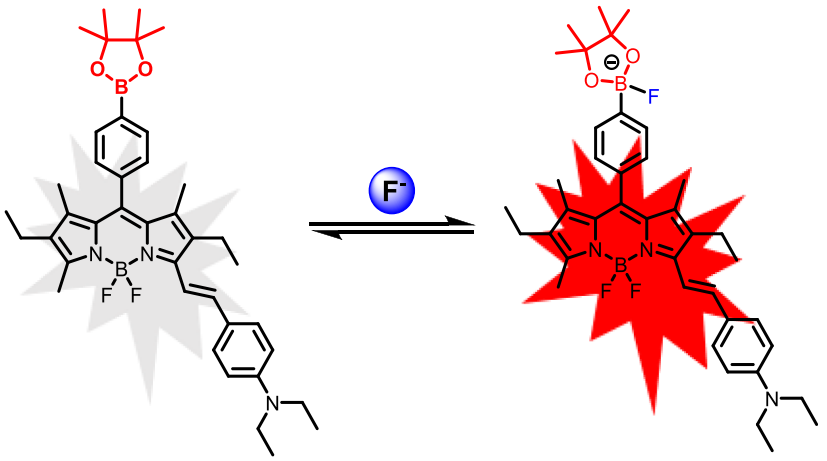

Scheme 2. Preparation of Probe BEB-F

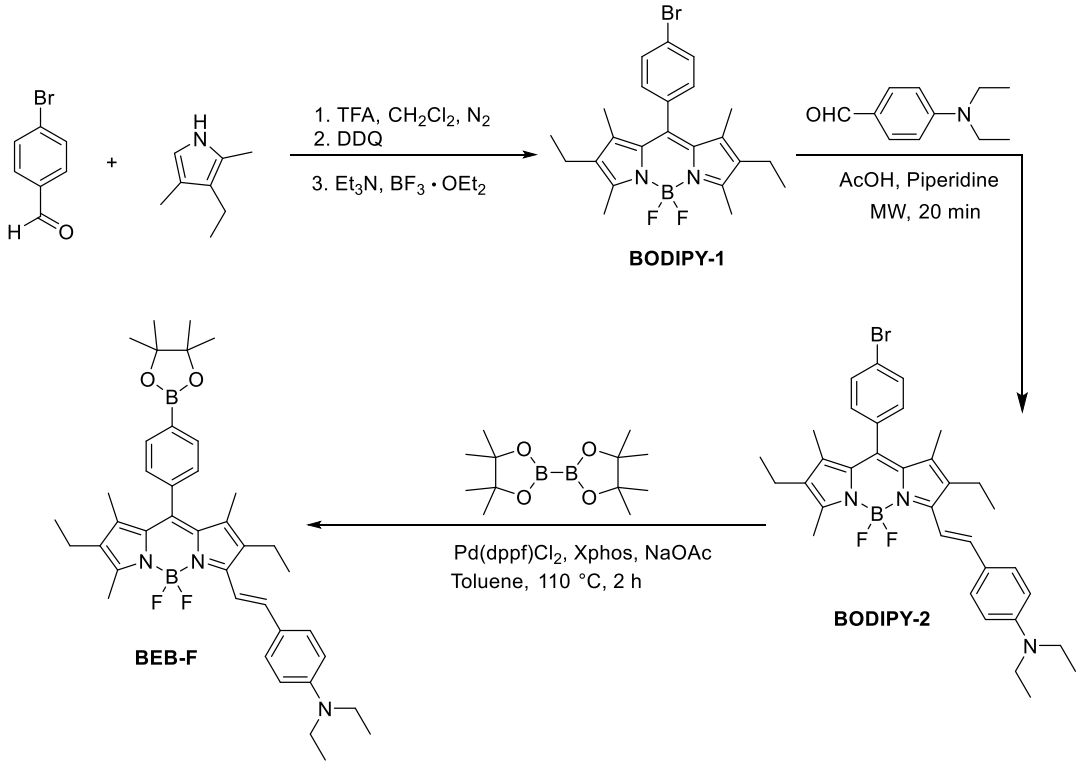

synthesized a novel 4,4-difluoro-4-bora-3a,4a-diaza-*s*-indacene (BODIPY) derivative bearing a pinacol boronate group for imaging F^- in aqueous solutions (Scheme 1). Microwave technology and palladium-catalyzed boronization borylation reactions were used in the synthesis of this probe molecule, which provides the advantages of both ease of operation and high product yield. The pinacol boronate group will bond to F^- and lead to borate anion, which results in a change in the absorption, emission properties, and fluorescence of the probe. Further experiments disclosed that it can be used for the real-time detection in vivo bioimaging of exogenous F^-.

2. RESULTS AND DISCUSSION

2.1. Synthesis of Probe BEB-F. A total of three steps are required for the synthesis of the target probe BEB-F, and the synthetic procedure is described in Scheme 2. First, 4-bromobenzaldehyde reacted with 3-ethyl-2,4-dimethyl-1H-pyrrole and subsequently complexed with $Et_2O{\cdot}BF_3$ in the presence of triethylamine to produce BODIPY-1. Then, for the second step of Knoevenagel condensation reaction between BODIPY-1 and *N*,*N*-diethylaminobenzaldehyde, we used microwave technology to facilitate this reaction, which has the advantage of not having by-products with similar polarity to the probe BEB-F and facilitates the isolation of high purity products. The unreacted raw material can also be separated and then recycled. In the third reaction step, the borylation of BODIPY-2 using $Pd(dppf)Cl_2$ as the catalyst and XPhos as the ligand afforded the probe BEB-F after careful column chromatography. All intermediate compounds and products were characterized by ^1H NMR, ^{13}C NMR, and high-resolution mass spectrometry (Figures S1−S9).

https://doi.org/10.1021/acsomega.2c03875
ACS Omega 2022, 7, 34317−34325

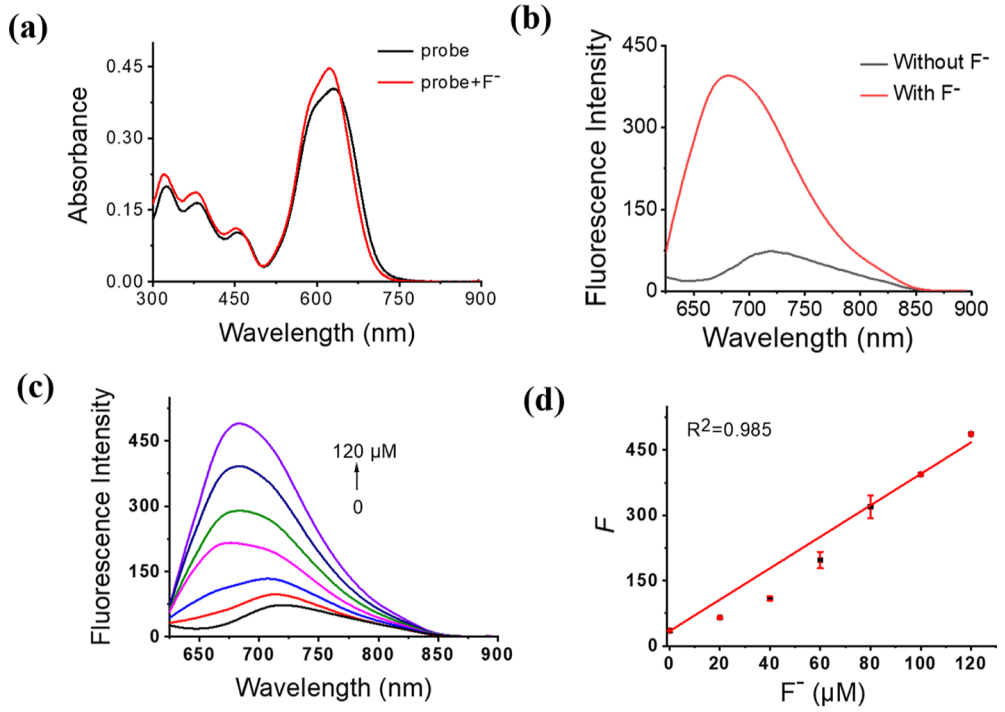

Figure 1. Absorption spectra (a) and fluorescence spectra (b) of BEB-F (10 μM) in pH 7.4 HEPES buffer (10 mM) with CTAB (100 μM) before and after reaction with F^- (100 μM) for 0.5 h. (c) Fluorescence response of the probe (10 μM) toward F^- at varied concentrations (0−120 μM) in pH 7.4 HEPES buffer (10 mM) with CTAB (100 μM). (d) Linear fitting curve of F against the concentration of F^-. $\lambda_{ex/em}$ = 600/677 nm.

2.2. Spectroscopic Property of Probe BEB-F and Its Response to F^-. The detection of aqueous solution with high sensitivity is a challenge. In this work, after careful screening, 100 μM cetyltrimethylammonium bromide (CTAB) was found to facilitate the detection of F^- by BEB-F in aqueous solution (Figure S10). Then, the UV−vis absorption spectra of BEB-F before and after the addition of F^- were measured in *N*-(2-hydroxyethyl)piperazine-*N*′-ethanesulfonic acid (HEPES) buffer (10 mM, pH = 7.4) with CTAB (100 μM). As shown in Figure 1a, BEB-F has an intense absorption peak at 630 nm, which slightly blue shifts after the addition of F^- to the solution. Next, the optimized excitation wavelength for fluorescence measurements was studied. As seen in Figure S11, without the addition of F^-, the fluorescence intensity of the probe BEB-F was essentially unchanged with different excitation wavelengths. At the same time, after the addition of F^- for 30 min, the fluorescence intensity of BEB-F gradually increased with the increase in excitation wavelength. To avoid scattered light interference from the excitation source, 600 nm was chosen as the excitation wavelength for the fluorescence measurements in this work. Under 600 nm excitation, an obvious enhancement of emission intensity at 677 nm was also observed after the addition of F^- (Figure 1b). To further investigate the interaction between BEB-F and F^-, the fluorescence titration experiment was carried out. As shown in Figure 1c, as anticipated, the fluorescence of BEB-F (10 μM) showed a large enhancement upon the addition of F^- (120 μM). In the range of 0−120 μM, the fluorescence intensity of probe BEB-F increases linearly with the concentration of fluoride ions. As displayed in Figure 1d, the relationship between the concentration of fluorine ion (x) and the fluorescence intensity (F) was obtained as follows: F = 33.99 + 3.61x (correlation coefficient R^2 = 0.9850). The detection limit (LOD) (3σ/slope, σ is the standard deviation of the blank measurement) was calculated to be 231 nM of F^-. The results indicated that the probe BEB-F can effectively detect F^- in aqueous solution. The photostability of probe BEB-F was studied by using laser irradiation (660 nm, 600 mW·cm^{-2}) as the light source, and the results indicate that the probe BEB-F exhibits good photostability (Figures S12 and S13).

2.3. Time-Dependence of BEB-F Response to F^-. The response time is an important parameter for evaluating the effectiveness of a probe. The response time of BEB-F to F^- was studied by a kinetic experiment (Figure 2). The result showed that the fluorescence intensity increased to its maximum in 10 min after adding F^- to the probe solution, which indicated that the probe instantly responds to F^-. In addition, the fluorescence intensity of the solution was stable for at least an hour after the reaction. Therefore, to obtain more accurate

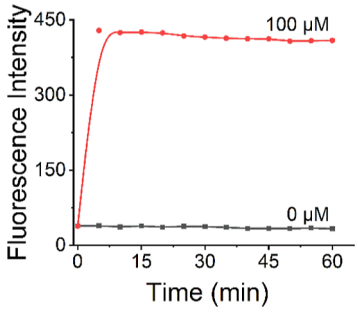

Figure 2. Reaction time on the fluorescence of BEB-F (10 μM) with varied concentrations (0 and 100 μM) of F^-. The fluorescence was measured in the pH 7.4 HEPES buffer (10 mM) with CTAB (100 μM). $\lambda_{ex/em}$ = 600/677 nm.

https://doi.org/10.1021/acsomega.2c03875
ACS Omega 2022, 7, 34317−34325

test results, we set the reaction time at 0.5 h in subsequent experiments.

2.4. pH Effect of BEB-F Response to F^-. The pH value is a crucial factor for evaluating the feasibility of fluorescent sensors for biological applications. We next examined the pH dependencies of the response of BEB-F to F^-. The results are shown in Figure 3, the probe BEB-F is stable, and the emission

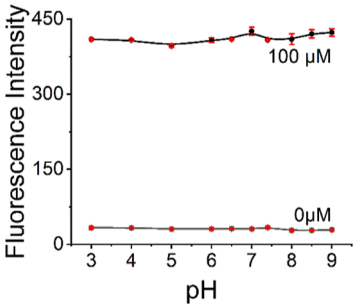

Figure 3. Effects of pH on the fluorescence of probe BEB-F (10 μM) with varied concentrations (0 and 100 μM) of F^-. The fluorescence was measured in the pH 7.4 HEPES buffer (10 mM) with CTAB (100 μM). $\lambda_{ex/em}$ = 600/677 nm.

is constant in a very wide range of pH 3.0−9.0. After the reaction of probe BEB-F and F^- for 0.5 h, the fluorescence intensity increased, and it was stable in the pH range of 3.0−9.0. The results suggested that the probe BEB-F can be used for the biological detection of F^-.

2.5. Selectivity of Probe BEB-F for F^-. To investigate the selectivity of the BEB-F for F^-, various anions such as Cl^-, Br^-, I^-, CH_3COO^-, ClO_4^-, HSO_4^-, $H_2PO_4^-$, NO_3^-, HPO_4^{2-}, OH^-, SO_4^{2-}, $ONOO^-$, ClO^-, and H_2O_2 were introduced into the system, the absorption (Figure S14) and fluorescence intensity (Figure 4a) of BEB-F did not change as compared with the blank signal. Furthermore, various cations (K^+, Mg^{2+}, Ca^{2+}, Zn^{2+}, Na^+, Cu^{2+}, Ni^{2+}, Co^{2+}, Al^{3+}, and Fe^{3+}) were also tested, which also did not cause significant changes in the absorption (Figure S15) and fluorescence of BEB-F (Figure 4b). Furthermore, the response experiments of the probe BEB-F in the presence of F^- in coexistence with other common ions were also carried out (Figures S16 and S17). The pinacol boronate group is widely reported as a recognition group for some ROS, such as $ONOO^-$, ClO^-, and H_2O_2. However, while examining the selectivity of probe BEB-F for F^-, no fluorescence response was found with the addition of these ROS for 30 min (Figure S18). However, after 1 h, the fluorescence intensity slightly decreased (Figure S18). We presume that the ROS may react with BEB-F and result in a non-fluorescent product. Anyway, such fluorescence turn-off responses are not significant and are quite slow, resulting in limited interference for the detection of F^-. All these results indicate that BEB-F was a highly selective probe for detecting F^-.

2.6. Cytotoxicity Assays. After confirming the good sensitivity and selectivity of BEB-F in detecting F^- in vitro, we went on to explore whether BEB-F could be useful in living cells. The cytotoxicity of BEB-F was first studied using the MTT assay. We incubated two experimental cells (HeLa cells and 4T1 cells) with different concentrations of BEB-F (0−50 μM) and then stained the cells with MTT to investigate the viability of the cells treated with BEB-F. Cytotoxicity studies in Figure 5 illustrated that cell viability was consistently above 85% even when the concentration of BEB-F was increased to 5 × 10^{-5} M. These results indicate that BEB-F has low cytotoxicity and good biocompatibility.

2.7. Imaging of Fluoride Ions in Live Cells. BEB-F was further used for imaging exogenous F^- in cells to explore its potential applications in studying bioimaging application. We examined the cell imaging ability of BEB-F in the presence of KF in HeLa cells and 4T1 cells using an inverted fluorescence imaging microscope. The results are shown in Figure 6; the BEB-F showed only a weak red fluorescence signal in the HeLa cells and 4T1 cells under the excitation of a green channel source. However, the fluorescence in the cells was significantly enhanced after being treated with KF in the medium, and the fluorescence rose with the increasing amount of F^-. These results illustrated that the BEB-F had excellent living cell imaging ability. As we learned from the literature, F^- above 1 mM results in osteoblast cytotoxicity, particularly to the nucleus and endoplasmic reticulum.[38] Neuronal cell lines exposed to ≥3 mM NaF undergo DNA damage, oxidative stress, mitochondrial agglutination, and cytoskeleton damage.[39,40] Owing to the high sensitivity and selectivity of the probe BEB-F, it remains potential for the application of BEB-F for F^- detection under some pathological conditions, which is our future work to be continued.

2.8. Detection of Fluoride Ions in Water Samples. BEB-F was also employed to determine F^- content in tap water and lake water samples. As shown in Table S2, BEB-F can detect F^- in the collected samples spiked with 80 and 100 μm F^- concentrations with the recovery close to 100%. In

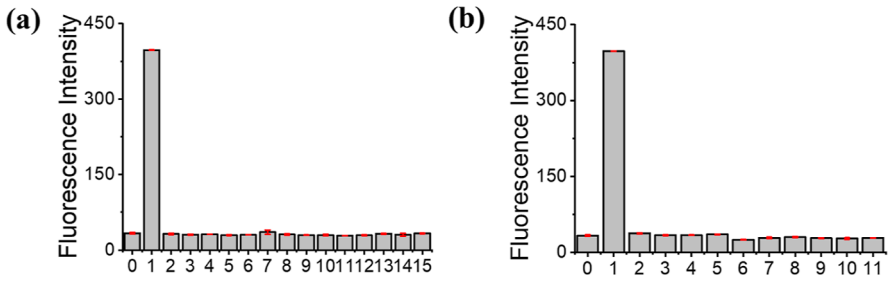

Figure 4. Fluorescence responses of 10 μM BEB-F toward various anions and cations. All experiments were performed in the pH 7.4 HEPES buffer (10 mM) with CTAB (100 μM). (a): (0) probe only; (1) 100 μM F^-; (2) 100 μM Cl^-; (3) 100 μM Br^-; (4) 100 μM I^-; (5) 100 μM CH_3COO^-; (6) 100 μM ClO_4^-; (7) 100 μM HSO_4^-; (8) 100 μM $H_2PO_4^-$; (9) 100 μM NO_3^-; (10) 100 μM HPO_4^{2-}; (11) 100 μM OH^-; (12) 100 μM SO_4^{2-}; (13) 100 μM H_2O_2; (14) 100 μM $ONOO^-$; and (15) 100 μM ClO^-. (b) (0) probe only; (1) 100 μM F^-; (2) 150 mM K^+; (3) 2.5 mM Mg^{2+}; (4) 2.5 mM Ca^{2+}; (5) 200 μM Zn^{2+}; (6) 100 mM Na^+; (7) 100 μM Cu^{2+}; (8) 100 μM Ni^{2+}; (9) 100 μM Co^{2+}; (10) 100 μM Al^{3+}; and (11) 100 μM Fe^{3+}. $\lambda_{ex/em}$ = 600/677 nm.

https://doi.org/10.1021/acsomega.2c03875
ACS Omega 2022, 7, 34317−34325

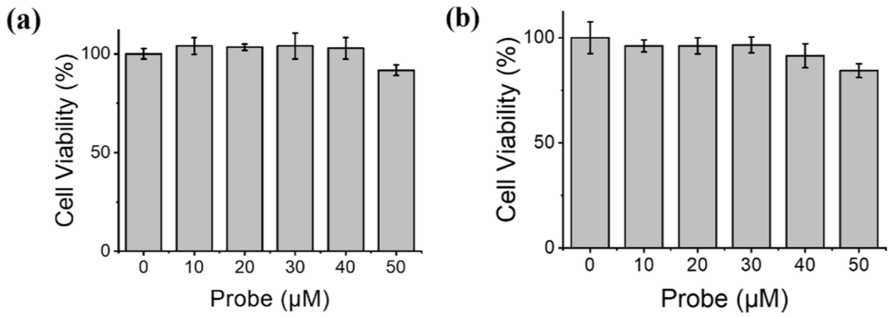

Figure 5. (a) Cell viability of HeLa treated with BEB-F. The viability of the cell without the probe is defined as 100%. The results are presented as mean ± standard deviation (n = 5). (b) Cell viability of 4T1 treated with the probe. The viability of the cell without the probe is defined as 100%. The results are presented as mean ± standard deviation (n = 5).

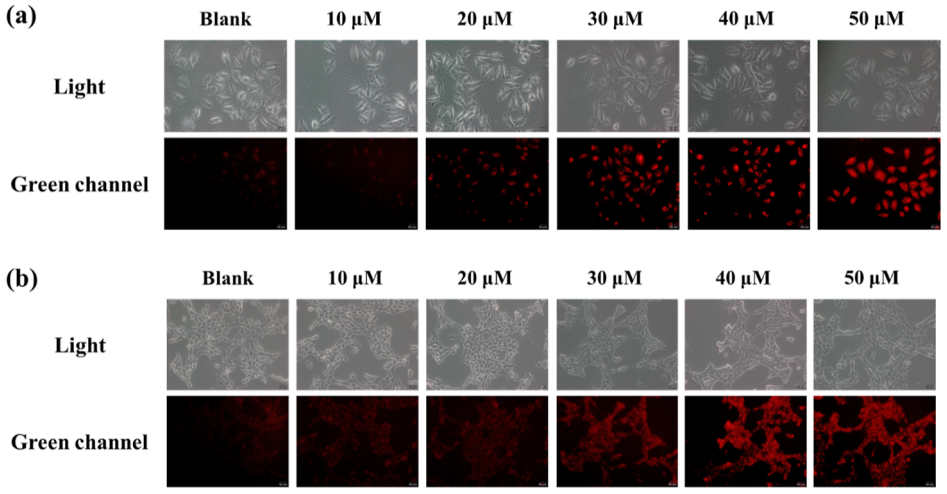

Figure 6. Fluorescence images of BEB-F in HeLa cells (a) and 4T1 cells (b) incubated with different concentrations of F^-. Fluorescence images of cells from the green channel (λ_{ex} = 460−550 nm). Scale bar: 20 μm.

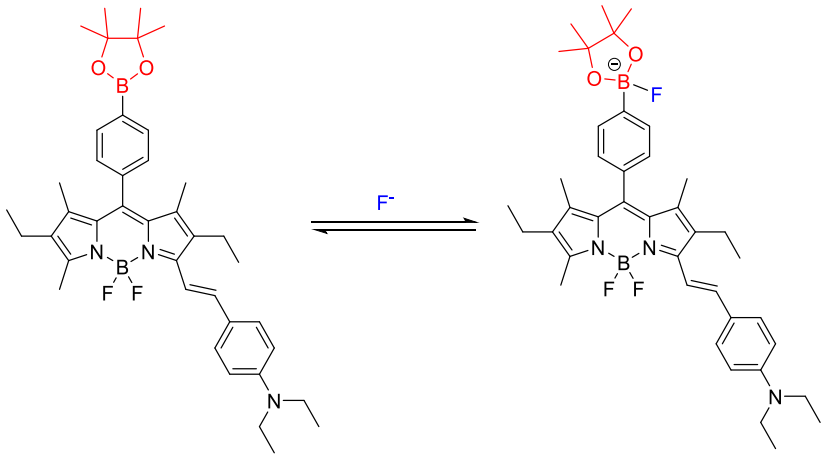

Figure 7. Proposed reaction mechanism of BEB-F with F^-.

addition, the fact that the compositions of tap water and lake water do not significantly interfere with F^- suggested the potential of utilizing this compound in water quality monitoring applications.

2.9. Reaction Mechanism of BEB-F with Fluoride Ions.

The mechanism of BEB-F with F^- was proposed in Figure 7. The boron atom of the boronic ester group has an sp^2 triangular planar geometry with an empty P orbital; after the addition of F^-, the boron center of the boronic ester is converted to sp^3 hybridization in the fluoroborate, thus leading to a significant perturbation of the p system and resulting in a response with a blueshift in the emission wavelength from 720 to 677 nm and an increase in fluorescence intensity.[41,42] We monitored the changes in ^{11}B NMR spectra produced via the addition of F^- to BEB-F solution. As shown in Figure 8, the boronate ester group exhibits a singlet at δ 21.65 ppm, and this singlet changes to 4.37 ppm, which was assigned to the boronic ester converted to sp^3 hybridization in the fluoroborate. Also, a

https://doi.org/10.1021/acsomega.2c03875
ACS Omega 2022, 7, 34317−34325

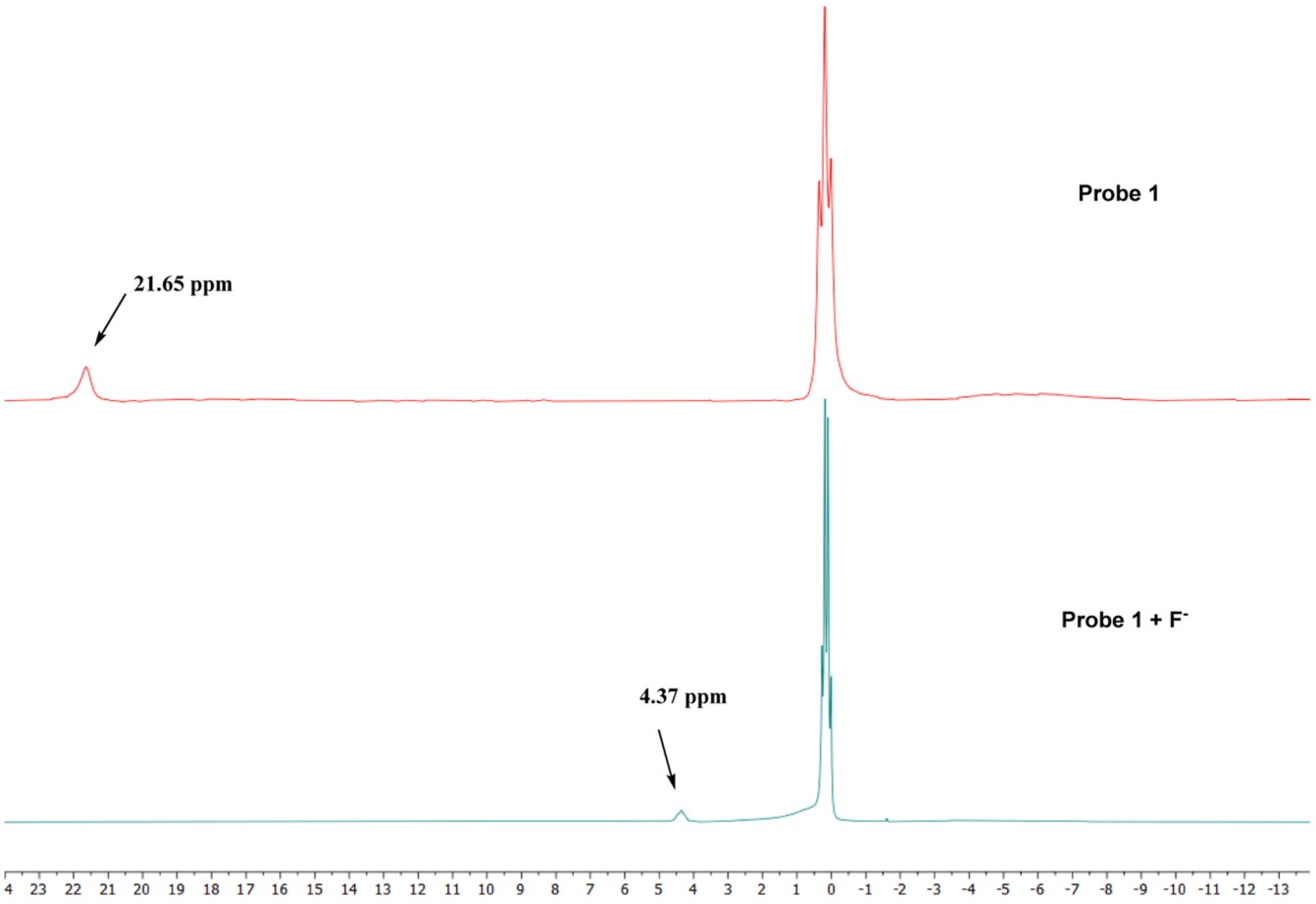

Figure 8. ^{11}B NMR spectra of BEB-F in the presence of fluoride anion.

new single peak at −123.87 ppm was observed by ^{19}F NMR after the addition of F^-, which is attributed to the new B−F bonding (Figure S19).

3. CONCLUSIONS

In summary, we have developed a BODIPY-based fluorescent probe, BEB-F, for the detection of fluoride ions in aqueous media. The probe synthesis was performed using microwave technology and a palladium-catalyzed efficient borylation reaction, which improved the yield of the product and facilitated the operation. Significantly, this probe BEB-F employing a pinacol borate group as the recognition moiety was capable of detecting fluoride ions in the aqueous phase, accompanied by a NIR fluorescence (at 677 nm) turn-on process. The probe BEB-F exhibited high selectivity and sensitivity for fluoride ions over other reactive cations and anions and has been demonstrated to have a linear response to fluoride ions with an LOD of 0.231 μM. Furthermore, this probe can be successfully utilized for detecting fluoride ions in real water samples and imaging those in HeLa cells and 4T1 cells. Therefore, this work provides a promising NIR probe for the rapid detection of fluoride ions found in environmental and biological samples.

4. MATERIALS AND METHODS

4.1. Materials and Instruments. Unless otherwise noted, all reagents and materials were commercially available and used without further purification. All aqueous solutions were prepared with deionized water, which was purified using a Nex Up 1000 (Human, South Korea). The human cervical cancer cells (HeLa cells) and mouse mammary cancer cells (4T1 cells) were obtained from the Key Laboratory of Basic Pharmacology, Zunyi Medical University. ^{1}H NMR and ^{13}C spectra were obtained on the Agilent 400 MHz-DD2 (Agilent, USA). High-resolution mass spectrometry (HR-MS) was obtained on the Agilent QTOF 6550 mass spectrometer. The UV−vis absorption spectra were obtained on a TU-1901 spectrometer (Persee, Beijing, China). The fluorescence spectrum measurements were performed on a Vary Eclipse spectrophotometer (Varian, USA) with the excitation and emission slit widths at 5 and 10 nm, respectively. The incubation was performed in the 3131 CO_2 incubator (Thermo, USA). Cytotoxicity was tested on WD-2102B (Liu Yi, Beijing, China). Fluorescence imaging experiments were performed on an Olympus fluorescent inverted microscope (IX73+DP73, Japan).

4.2. Synthesis and Characterization of BEB-F. The synthetic process for fluorescent BEB-F is displayed in Scheme 2.

4.2.1. Synthesis of BODIPY-1. Three drops of trifluoroacetic acid were added to a stirred solution of 4-bromobenzaldehyde (1.00 g, 5.40 mmol) and 3-ethyl-2,4-dimethyl-1*H*-pyrrole (1.82 mL, 13.51 mmol) in anhydrous CH_2Cl_2 (100 mL). The reaction mixture was stirred at r.t. under N_2 in a darkened flask overnight. Then, 2,3-dichloro-5,6-dicyano-1,4-benzoquinone (1.23 g, 5.40 mmol) was added in a single portion, and the mixture was stirred at r.t. for 6 h. Anhydrous triethylamine (4.51 mL, 32.43 mmol) was added to the mixture and stirred

https://doi.org/10.1021/acsomega.2c03875
ACS Omega 2022, 7, 34317−34325

at r.t. for 2 h. After that, $Et_2O{\cdot}BF_3$ (6.67 mL, 54.05 mmol) was added, and the mixture was stirred at r.t. overnight. Next, the reaction mixture was washed with brine (3 × 100 mL). The separated organic fractions were dried (Na_2SO_4) and filtered, and then the solvent was removed to yield a black/dark-violet residue with a green tint. The crude product was purified via chromatography over silica gel with a 20/1 (v/v) petroleum ether/ethyl acetate to provide a red powder (744.00 mg, yield 30%). ^{1}H NMR (400 MHz, $CDCl_3$): δ 7.63 (d, J = 8.2 Hz, 1H), 7.18 (d, J = 8.2 Hz, 1H), 2.53 (s, 3H), 2.30 (q, J = 7.5 Hz, 2H), 1.31 (s, 3H), 0.98 (t, J = 7.6 Hz, 3H). ^{13}C NMR (101 MHz, $CDCl_3$): δ 154.10, 138.11, 134.71, 132.98, 132.30, 130.47, 130.08, 122.97, 17.05, 14.63, 12.53, 11.95. HRMS (ESI-TOF, m/z): for $C_{23}H_{26}BBrF_2N_2$ $[M + H]^+$ calcd, 459.1419; found, 459.1439.

4.2.2. Synthesis of BODIPY-2. BODIPY-1 (700.00 mg, 1.52 mmol), *p-N,N*-diethylaminobenzaldehyde (324.24 mg, 1.83 mmol), piperidine (0.76 mL), acetic acid (0.76 mL), and 20 mL of dry toluene were added in a 50 mL glass tube sealed with a Teflon cap. The sample was irradiated at 200 W and 190 °C for 20 min in a CEM-Discover monomode microwave apparatus. After completion of the reaction, the mixture was directly poured into a silica gel column and eluted with a 15/1 (v/v) dichloromethane/petroleum ether to provide a blue powder (102.19 mg, yield 10%). ^{1}H NMR (400 MHz, $CDCl_3$): 7.63 (d, J = 8.2 Hz, 2H), 7.58−7.47 (m, 3H), 7.24−7.17 (m, 3H), 6.66 (d, J = 8.8 Hz, 2H), 3.40 (q, J = 6.9 Hz, 4H), 2.65−2.51 (m, 5H), 2.31 (q, J = 7.5 Hz, 2H), 1.37−1.24 (m, 6H), 1.22 − 1.13 (m, 9H), 0.99 (t, J = 7.5 Hz, 3H). ^{13}C NMR (101 MHz, $CDCl_3$): δ 152.95, 148.21, 138.58, 136.76, 135.19, 132.81, 132.21, 130.47, 129.09, 124.56, 122.85, 119.06, 114.74, 111.43, 44.49, 31.43, 30.15, 18.45, 17.12, 14.69, 14.00, 12.64, 11.93, 11.76. HRMS (ESI-TOF, m/z): for $C_{34}H_{39}BBrF_2N_3$ $[M + H]^+$ calcd, 618.2467; found, 618.2479.

4.2.3. Synthesis of BEB-F. BODIPY-2 (100.00 mg, 0.16 mmol), bis(pinacolato)diboron (61.59 mg, 0.24 mmol), sodium acetate anhydrous (53.06 mg, 0.24 mmol), and Pd(dppf)Cl_2 (11.83 mg, 0.02 mmol) were dissolved in toluene (5 mL) and stirred for 7 h at 110 °C. After the reaction mixture was cooled to room temperature, toluene was evaporated under reduced pressure. The residue was diluted with dichloromethane (20 mL), washed with saturated $NaHCO_3$ (10 mL × 3), and dried by Na_2SO_4; then, the solvent was removed and purified by chromatography over silica gel (petroleum ether/ethyl acetate = 10/1) to provide a blue powder (83.94 mg, yield 78%). ^{1}H NMR (400 MHz, $CDCl_3$): δ 7.89 (d, J = 7.6 Hz, 2H), 7.48 (d, J = 8.6 Hz, 3H), 7.31 (d, J = 7.5 Hz, 2H), 7.18 (d, J = 16.6 Hz, 1H), 6.66 (d, J = 8.4 Hz, 2H), 3.39 (d, J = 9.2 Hz, 4H), 2.58 (t, J = 8.1 Hz, 5H), 2.30 (q, J = 7.6 Hz, 2H), 1.40 (s, 12H), 1.27−1.25 (m, 6H), 1.19 (t, J = 7.1 Hz, 6H), 1.14 (t, J = 7.4 Hz, 3H), 0.98 (t, J = 7.5 Hz, 3H). ^{13}C NMR (101 MHz, $CDCl_3$): δ 148.11, 139.11, 136.34, 135.16, 128.99, 127.99, 124.68, 114.92, 111.45, 109.98, 103.62, 84.08, 44.47, 30.14, 29.69, 24.94, 24.82, 24.54, 18.42, 17.11, 14.66, 13.99, 12.63, 11.80, 11.61. HRMS (EI-TOF, m/z): for $C_{40}H_{51}B_2F_2N_3O_2$ $[M + H]^+$ calcd 666.4214; found, 666.4210.

4.3. General Procedures for Spectral Measurements. The stock solutions (3 mM) of tetrabutylammonium fluoride, $KHSO_4$, KH_2PO_4, NaClO, $NaNO_3$, Na_2HPO_4, NaOH, Na_2SO_4, NaCl, KBr, KI, CH_3COONa, $KClO_4$, H_2O_2, and ONOOH were prepared in deionized water. The stock solutions (3 mM) of KCl, $MgCl_2$, $CaCl_2$, $ZnCl_2$, NaCl, $AlCl_3$, $CuCl_2$, $CoCl_2$, $NiCl_2$, and $FeCl_3$ were prepared in deionized water. A stock solution of BEB-F (3 mM) was prepared in dimethyl sulfoxide; then, 10 μL of the stock solution was diluted with a mixed solution of CTAB containing HEPES buffer (10 mM, pH = 7.4), and different volume stock solutions (3 mM) of F^- were added until the total volume was 3 mL. Then, the final concentration of 10 μM BEB-F with 100 μM CTAB solution was used for F^- spectral measurement. The same amount of analyte is added to the probe test solutions for subsequent selective determination. Titration experiments are performed by adding different amounts of F^- to the probe solution and measuring optical changes. The reaction conditions were optimized with a certain amount of fluoride ions and probe.

4.4. Cytotoxicity Assay. The cytotoxicity of BEB-F was determined using MTT assays. HeLa cells and 4T1 cells were incubated in Dulbecco's modified Eagle medium (DMEM) supplemented with 10% FBS (fetal bovine serum) in an atmosphere of 5% CO_2 and 95% air at 37 °C. The cells were placed in a 96-well plate and incubated for 24 h upon different concentrations of BEB-F of 0.0, 10.0, 20.0, 30.0, 40.0, and 50.0 μM, respectively. Finally, the MTT assay followed. The cytotoxic effect (VR) of BEB-F was assessed using the following equation

$$VR = A/A_0 \times 100\%$$

where A and A_0 are the absorbance of the experimental group and control group using a microplate reader at 490 nm, respectively.

4.5. Living Cell Culture and Imaging. HeLa cells and 4T1 cells were incubated in DMEM supplemented with 10% FBS in an atmosphere of 5% CO_2 and 95% air at 37 °C. The cells were seeded in six-well flat-bottomed plates and incubated for 24 h before cell imaging. For the control experiment, the cells were incubated with a 10 μM probe for 0.5 h. Meanwhile, the other groups were incubated with different concentrations of F^- for 0.5 h and then treated with the 10 μM probe for another 0.5 h. Before imaging, all cells were washed three times with PBS buffer. All fluorescence images were acquired using an inverted fluorescence imaging microscope, and the fluorescence signals at the green field were collected.

■ ASSOCIATED CONTENT

Supporting Information

The Supporting Information is available free of charge at https://pubs.acs.org/doi/10.1021/acsomega.2c03875.

Additional experiment procedures, spectra (UV−vis absorption, fluorescence, NMR, and ESI-MS), imaging data, and full reference information (PDF)

■ AUTHOR INFORMATION

Corresponding Authors

Hongyu Li − *College of Pharmacy, Zunyi Medical University, Zunyi 563003, China; Key Laboratory of Basic Pharmacology of Ministry of Education and Joint International Research Laboratory of Ethnomedicine of Ministry of Education, Zunyi Medical University, Zunyi 563000, China; Guizhou International Scientific and Technological Cooperation Base for Medical Photo-Theranostics Technology and Innovative Drug Development, Zunyi 563003, China*; Email: lihongyu@iccas.ac.cn

https://doi.org/10.1021/acsomega.2c03875
ACS Omega 2022, 7, 34317−34325

Zeli Yuan − *College of Pharmacy, Zunyi Medical University, Zunyi 563003, China; Key Laboratory of Basic Pharmacology of Ministry of Education and Joint International Research Laboratory of Ethnomedicine of Ministry of Education, Zunyi Medical University, Zunyi 563000, China; Guizhou International Scientific and Technological Cooperation Base for Medical Photo-Theranostics Technology and Innovative Drug Development, Zunyi 563003, China;* orcid.org/0000-0001-5354-769X; Email: zlyuan@zmu.edu.cn

Xinmin Li − *College of Pharmacy, Zunyi Medical University, Zunyi 563003, China; Key Laboratory of Basic Pharmacology of Ministry of Education and Joint International Research Laboratory of Ethnomedicine of Ministry of Education, Zunyi Medical University, Zunyi 563000, China; Guizhou International Scientific and Technological Cooperation Base for Medical Photo-Theranostics Technology and Innovative Drug Development, Zunyi 563003, China;* orcid.org/0000-0003-1768-2370; Email: lixm@zmu.edu.cn

Authors

Yan Liu − *College of Pharmacy, Zunyi Medical University, Zunyi 563003, China; Key Laboratory of Basic Pharmacology of Ministry of Education and Joint International Research Laboratory of Ethnomedicine of Ministry of Education, Zunyi Medical University, Zunyi 563000, China; Guizhou International Scientific and Technological Cooperation Base for Medical Photo-Theranostics Technology and Innovative Drug Development, Zunyi 563003, China*

Yaping Zhou − *College of Pharmacy, Zunyi Medical University, Zunyi 563003, China*

Jie Gao − *College of Pharmacy, Zunyi Medical University, Zunyi 563003, China; Key Laboratory of Basic Pharmacology of Ministry of Education and Joint International Research Laboratory of Ethnomedicine of Ministry of Education, Zunyi Medical University, Zunyi 563000, China; Guizhou International Scientific and Technological Cooperation Base for Medical Photo-Theranostics Technology and Innovative Drug Development, Zunyi 563003, China*

Mingyan Yang − *College of Pharmacy, Zunyi Medical University, Zunyi 563003, China; Key Laboratory of Basic Pharmacology of Ministry of Education and Joint International Research Laboratory of Ethnomedicine of Ministry of Education, Zunyi Medical University, Zunyi 563000, China; Guizhou International Scientific and Technological Cooperation Base for Medical Photo-Theranostics Technology and Innovative Drug Development, Zunyi 563003, China*

Complete contact information is available at: https://pubs.acs.org/10.1021/acsomega.2c03875

Notes

The authors declare no competing financial interest.

■ ACKNOWLEDGMENTS

We are grateful for the financial support from the Guizhou Science and Technology Foundation ZK[2021]038, the National Natural Science Foundation of China (grant nos. 22267025, 22164022, 22065042), the Innovative Group Project of Guizhou Province of Education (KY[2018]024), the Excellent Youth Scientific Talents of Guizhou ([2021] 5638), the Talents of Guizhou Science and Technology Cooperation Platform ([2020]4104), and the Guizhou Science and Technology support plan ([2020]4Y158).

■ REFERENCES

(1) Jali, B.; Barick, A.; Mohapatra, P.; Sahoo, S. A comprehensive review on quinones based fluoride selective colorimetric and fluorescence chemosensors. *J. Fluorine Chem.* **2021**, *244*, 109744.
(2) Udhayakumari, D. Detection of toxic fluoride ion via chromogenic and fluorogenic sensing. A comprehensive review of the year 2015-2019. *Spectrochim. Acta, Part A* **2020**, *228*, 117817.
(3) Wang, L.; Ding, H.; Ran, X.; Tang, H.; Cao, D. Recent progress on reaction-based BODIPY probes for anion detection. *Dyes Pigm.* **2020**, *172*, 107857.
(4) Kleerekoper, M. The role of fluorlde in the prevention of osteoporosis. *Endocrinol Metab. Clin. N. Am.* **1998**, *27*, 441−452.
(5) Everett, E. Fluoride's effects on the formation of teeth and bones, and the influence of genetics. *J. Dent. Res.* **2011**, *90*, 552−560.
(6) Bharti, V. K.; Arup, G.; Krishna, K. Fluoride sources, toxicity and its amelioration: a review. *Ann. Environ. Sci. Toxicol.* **2017**, *2*, 21−32.
(7) Ullah, R.; Zafar, M.; Shahani, N. Potential fluoride toxicity from oral medicaments: a review. *Iran. J. Basic Med. Sci.* **2017**, *20*, 841−848.
(8) Kabir, H.; Gupta, A.; Tripathy, S. Fluoride and human health: systematic appraisal of sources, exposures, metabolism, and toxicity. *Crit. Rev. Environ. Sci. Technol.* **2020**, *50*, 1116−1193.
(9) Wei, Y.; Zeng, B.; Zhang, H.; Chen, C.; Wu, Y.; Wang, N.; Wu, Y.; Zhao, D.; Zhao, Y.; Iqbal, J.; Shen, L. Comparative proteomic analysis of fluoride treated rat bone provides new insights into the molecular mechanisms of fluoride toxicity. *Toxicol. Lett.* **2018**, *291*, 39−50.
(10) Zuo, H.; Chen, L.; Kong, M.; Qiu, L.; Lü, P.; Wu, P.; Yang, Y.; Chen, K. Toxic effects of fluoride on organisms. *Life Sci.* **2018**, *198*, 18−24.
(11) Han, J.; Zhang, J.; Gao, M.; Hao, H.; Xu, X. Recent advances in chromo-fluorogenic probes for fluoride detection. *Dyes Pigm.* **2019**, *162*, 412−439.
(12) Zhou, Y.; Zhang, J.; Yoon, J. Fluorescence and colorimetric chemosensors for fluoride-ion detection. *Chem. Rev.* **2014**, *114*, 5511−5571.
(13) Chen, P.; Bai, W.; Bao, Y. Fluorescent chemodosimeters for fluoride ions via silicon-fluorine chemistry: 20 years of progress. *J. Mater. Chem. C* **2019**, *7*, 11731−11746.
(14) Tian, X.; Murfin, L.; Wu, L.; Lewis, S.; James, T. Fluorescent small organic probes for biosensing. *Chem. Sci.* **2021**, *12*, 3406−3426.
(15) Wang, H.; Wang, X.; Li, P.; Dong, M.; Yao, S.; Tang, B. Fluorescent probes for visualizing ROS-associated proteins in disease. *Chem. Sci.* **2021**, *12*, 11620−11646.
(16) Singhal, P.; Jha, S. A semi quantitative visual probe for fluoride ion sensing in aqueous medium. *J. Lumin.* **2019**, *206*, 113−119.
(17) Yan, X.; Lan, H.; Li, Y.; Yan, X.; Xing, Q.; Wang, W.; Zhang, J.; Xiao, S. High-contrast colourimetric probes for fluoride and trace water based on tautomerization of naphthalimide and application in fingerprint imaging. *Spectrochim. Acta, Part A* **2021**, *254*, 119674.
(18) Arabahmadi, R. A selective chemosensor and fluorescence probe for relay recognition of cations and fluoride ions in aqueous media with logic gate function. *Talanta* **2019**, *194*, 119−126.
(19) Padhan, S.; Podh, M.; Sahu, P.; Sahu, S. Optical discrimination of fluoride and cyanide ions by coumarin-salicylidene based chromofluorescent probes in organic and aqueous medium. *Sens. Actuators, B* **2018**, *255*, 1376−1390.
(20) Zhou, K.; Ren, M.; Wang, L.; Li, Z.; Lin, W. A targetable fluorescent probe for real-time monitoring of fluoride ions in mitochondria. *Spectrochim. Acta, Part A* **2018**, *204*, 777−782.
(21) Chen, X.; Liu, Y. C.; Bai, J.; Fang, H.; Wu, F.-Y.; Xiao, Q. A "turn-on" fluorescent probe based on BODIPY dyes for highly selective detection of fluoride ions. *Dyes Pigm.* **2021**, *190*, 109347.

(22) Chen, C. H.; Gabbaï, F. Exploiting the strong hydrogen bond donor properties of a borinic acid functionality for fluoride anion recognition. *Angew. Chem., Int. Ed.* **2018**, *57*, 521−525.
(23) Lee, H.; Jana, S.; Kim, J.; Lee, S.; Lee, M. Donor-acceptor-appended triarylboron Lewis acids: ratiometric or time-resolved turn-on fluorescence response toward fluoride binding. *Inorg. Chem.* **2020**, *59*, 1414−1423.
(24) Ranjith Kumar, J.; Rami Reddy, E.; Trivedi, R.; Vardhaman, A.; Giribabu, L.; Mirzadeh, N.; Bhargava, S. Isophorone-boronate ester: a simple chemosensor for optical detection of fluoride anion. *Appl. Organomet. Chem.* **2019**, *33*, No. e4688.
(25) Tao, T.; Zhao, J.; Chen, H.; Mao, S.; Yu, J.; Huang, W. Precisely controlling fluorescence enhancement and high-contrast colorimetric assay in OFF-ON fluoride sensing based on a diketopyrrolopyrrole boronate ester. *Dyes Pigm.* **2019**, *170*, 107638.
(26) Fang, H.; Gan, Y.; Wang, S.; Tao, T. A selective and colorimetric chemosensor for fluoride based on dimeric azulene boronate ester. *Inorg. Chem. Commun.* **2018**, *95*, 17−21.
(27) Galbraith, E.; James, T. Boron based anion receptors as sensors. *Chem. Soc. Rev.* **2010**, *39*, 3831−3842.
(28) Wade, C.; Broomsgrove, A.; Aldridge, S.; Gabbaï, F. Fluoride ion complexation and sensing using organoboron compounds. *Chem. Rev.* **2010**, *110*, 3958−3984.
(29) Wu, D.; Chen, L.; Lee, W.; Ko, G.; Yin, J.; Yoon, J. Recent progress in the development of organic dye based near-infrared fluorescence probes for metal ions. *Coord. Chem. Rev.* **2018**, *354*, 74−97.
(30) Li, J. B.; Liu, H. W.; Fu, T.; Wang, R.; Zhang, X.-B.; Tan, W. Recent progress in small-molecule Near-IR probes for bioimaging. *Trends Chem.* **2019**, *1*, 224−234.
(31) Du, M.; Huo, B.; Liu, J.; Li, M.; Fang, L.; Yang, Y. A near-infrared fluorescent probe for selective and quantitative detection of fluoride ions based on Si-Rhodamine. *Anal. Chim. Acta* **2018**, *1030*, 172−182.
(32) Shen, Y.; Zhang, X.; Zhang, Y.; Li, H.; Chen, Y. An ICT-Modulated strategy to construct colorimetric and ratiometric fluorescent sensor for mitochondria-targeted fluoride ion in cell living. *Sens. Actuators, B* **2018**, *258*, 544−549.
(33) Xu, X.; Chen, W.; Yang, M.; Liu, X.-J.; Wang, F.; Yu, R.-Q.; Jiang, J.-H. Mitochondrial-targeted near-infrared fluorescence probe for selective detection of fluoride ions in living cells. *Talanta* **2019**, *204*, 655−662.
(34) Li, L.; Zhang, M.; Ding, L.; Ren, G.; Hou, X.; Liu, W.; Wang, H.; Wang, B.; Yan, L.; Diao, H. Ultrafast fluorescent probe with near-infrared analytical wavelength for fluoride ion detection in real samples. *Spectrochim. Acta, Part A* **2021**, *252*, 119518.
(35) Li, Y.; Sun, Q.; Su, L.; Yang, L.; Zhang, J.; Yang, L.; Liu, B.; Jiang, C.; Zhang, Z. A single nanofluorophore "turn on" probe for highly sensitive visual determination of environmental fluoride ions. *RSC Adv.* **2018**, *8*, 8688−8693.
(36) Yu, X.; Yang, L.; Zhao, T.; Zhang, R.; Yang, L.; Jiang, C.; Zhao, J.; Liu, B.; Zhang, Z. Multicolorful ratiometric-fluorescent test paper for determination of fluoride ions in environmental water. *RSC Adv.* **2017**, *7*, 53379−53384.
(37) Chansaenpak, K.; Kamkaew, A.; Weeranantanapan, O.; Suttisintong, K.; Tumcharern, G. Coumarin probe for selective detection of fluoride ions in aqueous solution and its bioimaging in live cells. *Sensors* **2018**, *18*, 2042.
(38) Qu, W.-J.; Zhong, D.-B.; Wu, P. F.; Wang, J.-F.; Han, B. Sodium fluoride modulates caprine osteoblast proliferation and differentiation. *J. Bone Miner. Metabol.* **2008**, *26*, 328−334.
(39) Johnston, N.; Strobel, S. Principles of fluoride toxicity and the cellular response: a review. *Arch. Toxicol.* **2020**, *94*, 1051−1069.
(40) Zhang, M.; Wang, A.; Xia, T.; He, P. Effects of fluoride on DNA damage, S-phase cell-cycle arrest and the expression of NF-kappaB in primary cultured rat hippocampal neurons. *Toxicol. Lett.* **2008**, *179*, 1−5.
(41) López-Alled, C. M.; Sanchez-Fernandez, A.; Edler, K.; Sedgwick, A.; Bull, S.; McMullin, C.; Kociok-Köhn, G.; James, T.; Wenk, J.; Lewis, S. Azulene-boronate esters: colorimetric indicators for fluoride in drinking water. *Chem. Commun.* **2017**, *53*, 12580−12583.
(42) Kim, Y.; Gabbaï, F. Cationic boranes for the complexation of fluoride ions in water below the 4 ppm maximum contaminant level. *J. Am. Chem. Soc.* **2009**, *131*, 3363−3369.

https://doi.org/10.1021/acsomega.2c03875
ACS Omega 2022, 7, 34317−34325